Transient Amplification of Broken Symmetry in Elastic Snap-Through

Qiong Wang,[1,*] Andrea Giudici,[2,*] Weicheng Huang,[3] Yuzhe Wang,[4] Mingchao Liu,[2,5,6] Sameh Tawfick,[1] and Dominic Vella[2,†]

[1]Department of Mechanical Science and Engineering, University of Illinois at Urbana-Champaign, Urbana, Illinois 61801, USA
[2]Mathematical Institute, University of Oxford, Woodstock Rd, Oxford OX2 6GG, United Kingdom
[3]School of Engineering, Newcastle University, Newcastle upon Tyne NE1 7RU, United Kingdom
[4]Singapore Institute of Manufacturing Technology, Agency for Science, Technology and Research, Singapore, 138634, Singapore
[5]School of Mechanical and Aerospace Engineering, Nanyang Technological University, Singapore 639798, Singapore
[6]Department of Mechanical Engineering, University of Birmingham, Birmingham B15 2TT, United Kingdom

(Received 22 December 2023; accepted 23 May 2024; published 26 June 2024)

A snap-through bifurcation occurs when a bistable structure loses one of its stable states and moves rapidly to the remaining state. For example, a buckled arch with symmetrically clamped ends can snap between an inverted and a natural state as the ends are released. A standard linear stability analysis suggests that the arch becomes unstable to asymmetric perturbations. Surprisingly, our experiments show that this is not always the case: symmetric transitions are also observed. Using experiments, numerics, and a toy model, we show that the symmetry of the transition depends on the rate at which the ends are released, with sufficiently fast loading leading to symmetric snap-through. Our toy model reveals that this behavior is caused by a region of the system's state space in which any initial asymmetry is amplified. The system may not enter this region when loaded fast (hence remaining symmetric), but will traverse it for some interval of time when loaded slowly, causing a transient amplification of asymmetry. Our toy model suggests that this behavior is not unique to snapping arches, but rather can be observed in dynamical systems where both a saddle-node and a pitchfork bifurcation occur in close proximity.

DOI: 10.1103/PhysRevLett.132.267201

The rapidity of elastic snap-through is striking: just as the snapping shut of the venus flytrap's leaves catches its prey by surprise [1], the jumping disc and variants remain popular toys [2–4]. Nevertheless, detailed analysis has shown that the early dynamics of snap-through may be slower, and last longer, than naively expected—critical slowing-down is observed as the threshold for snap-through is approached [5,6], while dynamic changes close to threshold lead to a "delayed" snap-through [7].

The surprising features of dynamic snap-through result from the underlying bifurcation structure, which is itself sensitively dependent on the underlying symmetries of the problem, particularly the imposed boundary conditions [8,9]. The symmetry (or asymmetry) of the snap-through transition has also been shown to be controlled by geometrical parameters such as the aspect ratio (thickness-to-length) of a buckled beam [4,10]. However, recent experiments that used the rapidity of snap-through to initiate jumping in an insect-sized robot [11] also suggested that whether snap-through occurs symmetrically or asymmetrically may vary within the same experimental system (i.e., with the same geometrical and mechanical properties). This contradicts standard linear stability analyses, which suggests that snap-through should happen asymmetrically [12]. Understanding the origins (or absence) of asymmetry has important implications for controlling the jumps of these robots (e.g., whether they jump vertically or sideways), but is more generally important in applications of dynamic snap-through [13].

In this Letter, we study the snap-through that powered the jumping of insect-scale robots using a model system: a strip of spring steel (wear-resistant 1095 Spring Steel strip, modulus $E \approx 200$ GPa, thickness $b = 0.05$ mm, width $w = 25$ mm) of length $L = 108$ mm was formed into an arch by clamping its ends symmetrically at an angle $\alpha = \pi/12$ rad to the horizontal and imposing an end-shortening ΔL on one side [see Fig. 1(a)]. Given a clamping angle $\alpha > 0$ and sufficiently large values of $\Delta L/L$ the arch can exist in one of two (symmetric) states: the "natural" state (resembling a "Λ") and an "inverted" state (resembling an "M")—it is bistable [12]. However, as ΔL decreases, the inverted state ceases to exist and the system is forced to snap to the natural state. We vary ΔL experimentally by fixing one clamp while the other is

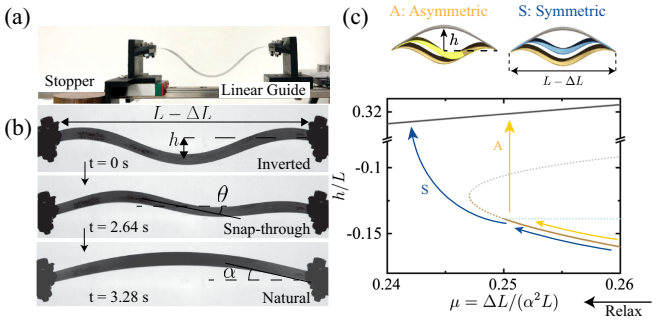

FIG. 1. (a) Experimental setup in which the ends of a steel strip (length L) are clamped at angle α to the horizontal. The clamp on the right is fixed while that on the left is moved along a linear guide by a motorized stage. (The stopper prevents overstretching after snap-through.) (b) Three snapshots of snap-through: an initial end-end compression ΔL is applied, allowing buckling in the inverted state (top). As ΔL is slowly decreased, the arch snaps from the inverted state to the natural state (bottom). The angle of inclination at the center $\theta(t)$ highlights asymmetry. (c) Bifurcation diagram showing stable equilibria as solid curves: the natural state (black) always exists while the inverted state (brown) vanishes at $\mu = \mu_* \approx 0.247$ but becomes unstable (dashed curve) for $\mu_* \le \mu < \mu_A = 1/4$ because of the presence of an unstable asymmetric mode (cyan dashed line). This complexity gives two routes to snap-through from the inverted to natural states: a symmetric path (blue arrow) and an asymmetric path (gold arrow).

attached to a motorized linear stage. The speed $|\dot{\Delta L}|$ can be controlled in the range 1 mm $s^{-1} \le |\dot{\Delta L}| \le 300$ mm s^{-1}.

"Snap-through" is captured via a high-speed movie (taken at 2245 fps) [14]. The images in Fig. 1(b) show that, at least in some circumstances, the arch may snap-through asymmetrically: the inclination angle at the center, $\theta(t)$, differs visibly from zero. Quantitative plots of $\theta(t)$ are shown in Fig. 2(a) and highlight that when ΔL is changed slowly, an initially small θ is significantly amplified close to the snap-through transition. Surprisingly, however, this is different when the motion is driven "quickly": for larger $|\dot{\Delta L}|$, θ does not increase significantly.

As a first indication of the root of this rich phenomenology, a bifurcation analysis [14] reveals several important insights. First, for sufficiently small values of $\alpha > 0$, the behavior of the system is controlled by the parameter

$$\mu = \frac{1}{\alpha^2}\frac{\Delta L}{L}, \tag{1}$$

which compares the typical angle induced by compression, $(\Delta L/L)^{1/2}$, to the clamping angle, α. A static analysis reveals that for $\mu < \mu_* \approx 0.247\ldots$ the natural state remains as an equilibrium but the inverted state vanishes via a saddle-node bifurcation at $\mu = \mu_*$. A standard linear stability analysis [12,14] also shows that at $\mu = \mu_A = 1/4 > \mu_*$ the inverted state becomes unstable and, further, that (linear) instability progresses via a growing asymmetric mode. This behavior, summarized in Fig. 1(c), leads us to hypothesize that paths in phase space may be symmetric or asymmetric depending on the loading rate [shown schematically in Fig. 1(c)].

To test the robustness of the speed-dependent symmetry or asymmetry observed experimentally, we use numerical experiments with the planar discrete elastic rod method [17–19]. The physical parameters in simulations are selected to correspond to physical experiments; typical results are shown in Fig. 2(b) and confirm that significant asymmetry can be observed with perfectly symmetrical

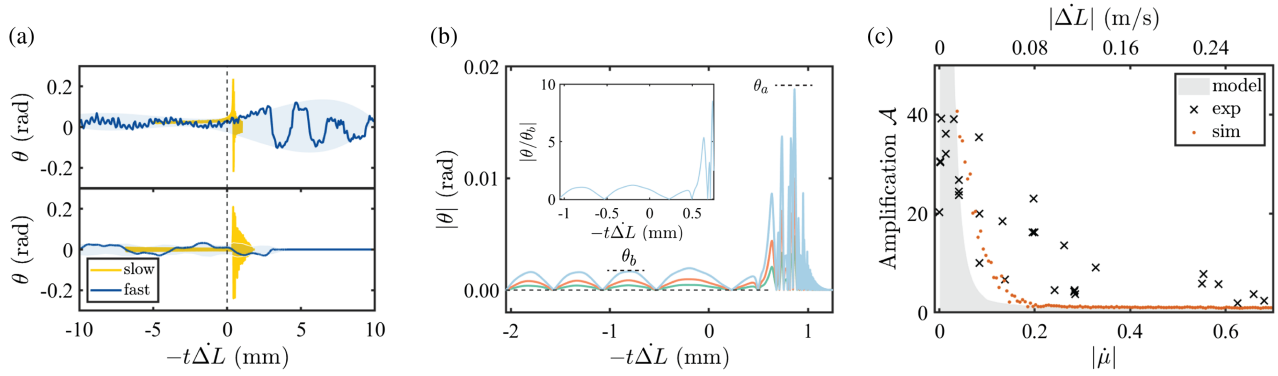

FIG. 2. Transient asymmetry in the snap-through of a symmetric arch. (a) Both the experimental (top) and simulation (bottom) results show that the central angle θ grows close to the snap-through transition at $t = 0$ (vertical dashed line), but only when the loading rate $|\dot{\Delta L}|$ is small enough. (In the slow case, $|\dot{\Delta L}| = 1.8$ mm/s; in the fast case, $|\dot{\Delta L}| = 246.6$ mm/s). The shaded region in each dataset shows the envelope of oscillations before and after snap-through. (b) Numerical simulations highlight the role of loading protocol: when both ends are moved with the same acceleration (dashed black line) the system remains perfectly symmetrical. With only one end moved (as in experiments), asymmetric oscillations are excited at low (green), medium (red), and high (blue) accelerations, and thus symmetry is broken. In each case, while the raw values of θ vary with the driving acceleration, plotting the amplification, collapses the curves (see inset). (c) The maximum amplification, defined in (2), shows a sensitive dependence on the loading rate $|\dot{\Delta L}|$ and its dimensionless equivalent, $\dot{\mu}$, in both experiments and simulations.

boundary conditions, but only with sufficiently small $|\dot{\Delta L}|$. Moreover, numerics show that small oscillations in θ are observed *before* snap-through; we call these precursor oscillations.

The numerical experiments show that small precursor oscillations are vital to asymmetry: when moving both ends perfectly symmetrically, no precursor oscillations are observed and the arch remains symmetric throughout snap-through [horizontal line in Fig. 2(c)]. However, moving just one end introduces small asymmetric precursor oscillations in the arch shape (despite the symmetric boundary conditions); these are then amplified during snap-through. Different accelerations excite precursor oscillations of different magnitude (and hence different raw asymmetries during snap-through), as might be expected. However, rescaling by the size of the oscillations before snap-through, $\theta_b = \max_{t<0}|\theta(t)|$, where $t = 0$ is defined such that $\mu(0) = \mu_*$, allows us to collapse these data [see inset of Fig. 2(c)]. This motivates measuring the amplification of asymmetry, defined as

$$\mathcal{A} := \frac{\max_{t>0}|\theta(t)|}{\max_{t<0}|\theta(t)|}. \tag{2}$$

(For the experiments, the oscillation amplitude is determined from the standard deviation of θ for $t < 0$ [14].) Both numerical and physical experiments show a distinct effect of the stretching rate $|\dot{\Delta L}|$ on $\mathcal{A}$: *the amount of amplification decreases with increasing end-stretching rate* $|\dot{\Delta L}|$ [Fig. 2(d)]. Both also pose a series of questions. First, why and how does the end-stretching rate determine the symmetry of the arch as it snaps through? Second, why is this transition observed as an amplification of an existing asymmetry?

A simple model to study snap-through instabilities is the von Mises truss [20,21]. However, the classic von Mises truss has only 1 degree of freedom and does not admit asymmetric modes. To capture asymmetry, we introduce the double-mass von Mises truss in which two masses are connected (via linear springs) to two rigid end points [see Fig. 3(a)]. With imposed end shortening, this system buckles either up or down to reduce the compression of the springs. To bias the system and ensure that one of these buckled states is preferred (the natural state), we include torsional springs between the clamps and the side springs whose relaxed position is at an angle α with respect to the horizontal. To stabilize the inverted state, we also include torsional springs connecting the central spring to its neighbors, penalizing deviations from flat—this introduces an effective bending stiffness.

A detailed analysis [14] shows that for small angles $\alpha \ll 1$ the state of the system can be described using two angles alone: the symmetric and asymmetric parts of the angles, denoted ψ_S and ψ_A, respectively. These angles are illustrated schematically in Fig. 3(a) (see [14] for formal

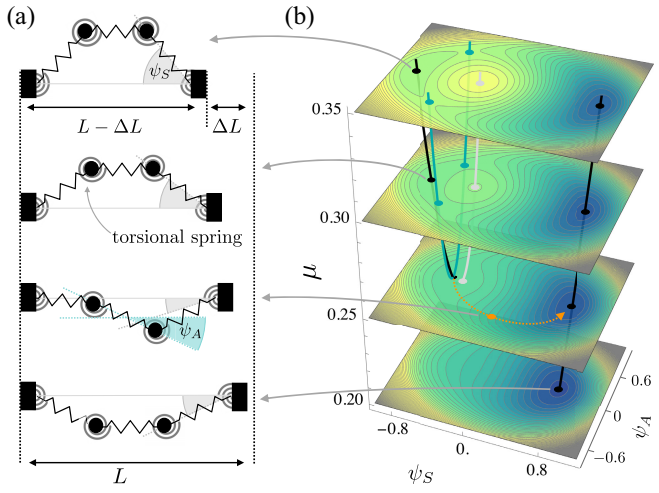

FIG. 3. (a) A sketch of the double-mass von Mises truss with torsional spring elements in various states, corresponding to the inverted arch (top) and the natural arch (bottom). (b) The evolution of the energy landscape as a function of the end-shortening parameter $\mu = \Delta L/(L\alpha^2)$.

definitions); loosely speaking, ψ_S corresponds to the height, h, of the corresponding arch while ψ_A is a measure of the asymmetry. For simplicity, we argue via symmetry in the main text, giving details of a formal analysis elsewhere [14]. Crucially, the angles $\psi_A, \psi_S \sim \alpha \ll 1$ while the relative end-shortening $\Delta L/L \sim \alpha^2$, again motivating the introduction of $\mu = \Delta L/(\alpha^2 L)$. Moreover, when $\alpha = 0$ we expect the energy to be even in ψ_S. However, the bias introduced by the clamps is linear in ψ_S (and independent of $\Delta L/L$); as such, there is an additional linear term in ψ_S. Similarly, the energy must be even in ψ_A, since the system is left-right symmetric. Thus, to fourth order in small quantities [i.e., at $O(\alpha^4)$], the energy takes the form

$$U = U_0 - a_1\psi_S + \frac{1}{2}(a_2 - a_3\mu)\psi_S^2 + \frac{1}{4}a_4\psi_S^4 + \frac{1}{2}f(\psi_S;\mu)\psi_A^2 + \frac{1}{4}b_4\psi_A^4, \tag{3}$$

where

$$f(\psi_S;\mu) = b_1 - b_2\mu + b_3\psi_S^2, \tag{4}$$

and $a_i, b_i > 0$ are constants that depend on the initial geometry and mechanical properties of the system [14]. The energy in Eq. (3) can be derived from first principles by summing the energies stored in the linear and torsional springs as functions of the masses' positions subject to a constraint on the total end displacement. Taking the leading order terms in small clamp angle, α, yields Eq. (3) [14]. Equation (3) shows that the coefficients of the two quadratic terms are not constant: the coefficient of ψ_S^2

varies with μ (as must be the case for a bifurcation to occur) while the coefficient of ψ_A^2 depends on ψ_S and μ.

The energy U is plotted as a function of μ, ψ_S, and ψ_A in Fig. 3(b). When μ is large, the system has 2 stable equilibria (black points), corresponding to the natural (global minimum) and inverted (local minimum) symmetric states. There are three more equilibria corresponding to a symmetric local maximum (gray) and two asymmetric saddles (cyan). As μ decreases, the two asymmetric saddles annihilate when $f(\psi_S;\mu)=0$ at a critical $\mu=\mu_A^{\mathrm{vM}}$. For $\mu<\mu_A^{\mathrm{vM}}$, the inverted equilibrium goes from being a minimum to being a saddle—it becomes susceptible to asymmetric perturbations. Moreover, when $\mu=\mu_*^{\mathrm{vM}}=a_2/a_3+3(2a_1^2a_4)^{1/3}/2a_3$, the inverted equilibrium is annihilated simultaneously with the maximum at $\psi_S^*=(a_1/2a_4)^{1/3}$ in a saddle-node bifurcation; only the natural symmetric equilibrium exists for $\mu<\mu^*$. Therefore, as μ decreases, the inverted equilibrium first becomes unstable to asymmetric perturbations before ceasing to exist altogether. This model replicates the bifurcation structure of the continuous arch [see Fig. 1(c)] but does so with only two variables, (ψ_S,ψ_A), rather than the continuous arch shape. Furthermore, by appropriate choice of two parameters (corresponding to the stiffness ratio of the torsional and linear springs and the length ratio of the central and edge springs), the two bifurcation points can be tuned to match those of the continuous arch—we ensure that $\mu_*^{\mathrm{vM}}=\mu_*\approx 0.247$ and $\mu_A^{\mathrm{vM}}=\mu_A=1/4$ and omit the superscript $^{\mathrm{vM}}$ henceforth.

To understand the dynamic behavior, and further quantify the energetic picture above, we use a variational approach to derive equations for the evolution of ψ_S and ψ_A. Ignoring higher order terms and rescaling time by the period of oscillations, $t_{\mathrm{osc}}[m/(\alpha^2 k)]^{1/2}$, where $t_{\mathrm{osc}}=9.477$ [14], the kinetic energy of the system can be written as $T=\dot{\psi}_S{}^2+\frac{1}{4}\dot{\psi}_A{}^2$, with differing prefactors between the translational energy of the center of mass and the rotational energy [14]. A standard application of the Euler-Lagrange equations then gives that, for $\psi_A\ll 1$

$$\ddot{\psi}_S/t_{\mathrm{osc}}^2=\frac{1}{2}a_1-\frac{1}{2}(a_2-a_3\mu)\psi_S-\frac{1}{2}a_4\psi_S^3, \tag{5}$$

$$\ddot{\psi}_A/t_{\mathrm{osc}}^2=-2f(\psi_S;\mu)\psi_A. \tag{6}$$

The system of equations (5)–(6) yield considerable insight. First, Eq. (6) illustrates a one-way coupling from ψ_S to ψ_A: the evolution of ψ_A depends on ψ_S but ψ_S evolves independently of ψ_A. More importantly, the equilibrium value of the function $f(\psi_S;\mu)$, in Eq. (6), changes sign when $\mu=\mu_A=1/4$. For $\mu>\mu_A$, any small ψ_A exhibits simple harmonic motion; for $\mu<\mu_A$ the oscillatory behavior of ψ_A changes to exponential growth and the symmetric equilibrium, $\psi_A=0$, is unstable. Moreover, Eq. (5) loses a pair of equilibrium solutions (a saddle-node bifurcation [22]) at $\mu=\mu_*\approx 0.247$. This reproduces the bifurcation picture in Fig. 1(c).

The change in behavior as f changes sign in Eq. (6) explains our observation that asymmetry in the initial conditions is amplified. Since amplification only occurs within the region of parameter space for which $f(\psi_S;\mu)<0$, we refer to this region as the *amplification region*—shown as the shaded region in the top panel of Fig. 4(a). Whether a trajectory enters the amplification region depends on the evolution of ψ_S, which is governed by (5) and depends not only on t and the instantaneous value of μ, but also on the rate at which μ changes, $|\dot{\mu}|$. We write

$$\mu=\mu_*-|\dot{\mu}|t$$

where t is the rescaled time and highlight that $\psi_S=\psi_S(t;|\dot{\mu}|)$. For small $|\dot{\mu}|$, the trajectory passes very close to the equilibrium solution, effectively evolving quasistatically with only a rapid change in ψ_S as oscillations in ψ_A give way to exponential growth. For larger values of $|\dot{\mu}|$, however, the trajectory passes further off the equilibrium path and the fast change in ψ_S associated with snap-through occurs with $\mu<\mu_*\approx 0.247$—a phenomenon known as "delayed bifurcation" [7,23].

Crucially, the dependence of the trajectory on $|\dot{\mu}|$ affects whether the trajectory enters the amplification region at all: for small $|\dot{\mu}|$, trajectories *do* enter the amplification region [thick portion of the yellow or light trajectory in Fig. 4(a)] and a small initial value, $\psi_A(0)=\psi_A^0$, is amplified as the trajectory passes through the amplification region. For large $|\dot{\mu}|$, trajectories do *not* pass through the amplification region

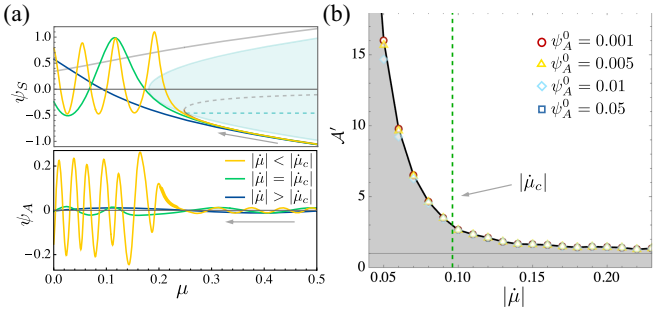

FIG. 4. (a) Trajectories of ψ_S and ψ_A for the double-mass von Mises truss model for different values of the loading rate $|\dot{\mu}|$ with an initial perturbation $\psi_A^0=0.01$. (Note that time goes from right to left here, since $\dot{\mu}<0$.) The blue shaded region highlights the amplification region in which $f(\psi_S;\mu)<0$: while a trajectory crosses this region, any asymmetry is amplified—see (6)—highlighted by thicker lines in the trajectory. This is observed only for $|\dot{\mu}|<|\dot{\mu}_c|$. (b) Numerical results for the fully nonlinear double-mass von Mises truss model show that results with different initial asymmetry can be collapsed by considering the maximum amplification $\mathcal{A}'\coloneqq\max|\psi_A|/|\psi_A^0|$ and that amplification only occurs for sufficiently slow loading, $|\dot{\mu}|<|\dot{\mu}_c|\approx 0.0961$ (vertical dashed line).

and ψ_A remains small throughout [dark blue trajectories in Fig. 4(a)]. This explains why there is a sharp change in behavior: significant asymmetry is observed only for sufficiently small $|\dot{\mu}|$.

To determine the critical value of $|\dot{\mu}|$, i.e., what we mean by sufficiently slow or fast, we must determine the value of $|\dot{\mu}|$ for which the trajectory just grazes the amplification region. The key result of this analysis [14] is that the critical value $|\dot{\mu}_c| \approx 0.0961$. This is compared with numerical results for the (full) system in Fig. 4(b)—points show the numerically observed amplification, while the prediction $|\dot{\mu}| = |\dot{\mu}_c|$ is shown by the vertical dashed line. As expected, the results show very little amplification for $|\dot{\mu}| > |\dot{\mu}_c|$. Moreover, Fig. 4(b) shows that for $|\dot{\mu}| < |\dot{\mu}_c|$ there is significant amplification of the underlying asymmetry, and hence an appreciable asymmetry develops. This can be understood heuristically as resulting from the transient nature of the amplification: asymmetry is only amplified while the trajectory passes through the amplification region. Trajectories with small $|\dot{\mu}|$ spend longer passing through this region, and hence experience greater amplification. One subtlety is that the phase of oscillation as snap-through occurs plays a role in determining the precise degree of amplification that is observed [14]. Hence, the shaded region in Figs. 2(c) and 4(b) show the range of amplifications possible as the phase varies.

In this Letter, we have presented experimental and numerical evidence that elastic snap-through may take place symmetrically or asymmetrically depending on the rate at which the system is driven through the snap-through transition. The double-mass von Mises truss model we have presented is thus able to capture the key physics that governs the behavior of a snapping arch observed in experiments and numerics. In particular, it shows that the asymmetry observed is caused by the transient amplification of a small initial asymmetric perturbation. Further, the model shows that this amplification occurs only when the dynamic loading is slow enough that the trajectory of the system passes through an *amplification zone*, thereby explaining the sharp transition in behavior that is observed at a critical loading rate $|\dot{\mu}_c|$. Qualitatively the results of this toy model agree with the experimental and numerical results [compare Figs. 2(d) and 4(b)].

The behavior we have reported in this Letter is general: it occurs whenever a system has both a saddle-node and a pitchfork bifurcation, since then its energy has the structure of (3), specifically a term quadratic in ψ_A whose prefactor depends on ψ_S. The amplification of the variable associated with the pitchfork bifurcation (ψ_A in our example), depends entirely on f and can be observed provided the analog of $f < 0$ at the saddle-node point μ_* for some values of ψ_S. The behavior of such systems close to the bifurcation point cannot be understood from a simple linear stability analysis—*how* the instability develops depends on fundamentally nonlinear phenomena. The generic nature of the transient amplification of asymmetry suggests the use of snap-through stimulation *rate* for control of elastic instabilities. For example, in the snap-induced jumping of robots [11], the ability to controllably switch snap-through between symmetric and asymmetric modes may lead to the ability to switch between vertical and forwards jumps.

Our numerics and toy model focus on the situation in which the boundary conditions are perfectly symmetric. However, in any experiment or application, small defects or imperfections are unavoidable. For small defects, the picture we have presented here persists, while for larger defects the rate of loading plays a slightly different role [24].

This work was partially supported by the UK Engineering and Physical Sciences Research Council via Grant No. EP/W016249/1 (D. V.). Q. W., Y. W., and S. T. acknowledge support from the Defense Advanced Research Projects Agency DARPA SHRIMP HR001119C0042. W. H. acknowledges the start-up funding from Newcastle University, UK. M. L. acknowledges support via start-up funding from the University of Birmingham. We are grateful to Michael Gomez for discussions.

*These authors contributed equally to this letter.
†dominic.vella@maths.ox.ac.uk

[1] Y. Forterre, J. M. Skotheim, J. Dumais, and L. Mahadevan, How the venus flytrap snaps, Nature (London) **433**, 421 (2005).
[2] C. Isenberg, The jumping disc, Phys. Educ. **22**, 158 (1987).
[3] C. Ucke and H. Schlichting, Revival of the jumping disc, Phys. Educ. **44**, 612 (2009).
[4] A. Pandey, D. E. Moulton, D. Vella, and D. P. Holmes, Dynamics of snapping beams and jumping poppers, Europhys. Lett. **105**, 24001 (2014).
[5] M. Gomez, D. E. Moulton, and D. Vella, Critical slowing down in purely elastic snap-through instabilities, Nat. Phys. **5**, 142 (2017).
[6] T. G. Sano and H. Wada, Twist-induced snapping in a bent elastic rod and ribbon, Phys. Rev. Lett. **122**, 114301 (2019).
[7] M. Liu, M. Gomez, and D. Vella, Delayed bifurcation in elastic snap-through instabilities, J. Mech. Phys. Solids **151**, 104386 (2021).
[8] B. Radisson and E. Kanso, Elastic snap-through instabilities are governed by geometric symmetries, Phys. Rev. Lett. **130**, 236102 (2023).
[9] B. Radisson and E. Kanso, Dynamic behavior of elastic strips near shape transitions, Phys. Rev. E **107**, 065001 (2023).
[10] P. S. Harvey and L. N. Virgin, Coexisting equilibria and stability of a shallow arch: Unilateral displacement-control experiments and theory, Int. J. Solids Struct. **54**, 1 (2015).
[11] Y. Wang, Q. Wang, M. Liu, Y. Qin, L. Cheng, O. Bolmin, M. Alleyne, A. Wissa, R. H. Baughman, D. Vella, and S. H. Tawfick, Insect-scale jumping robots enabled by a dynamic buckling cascade, Proc. Natl. Acad. Sci. U.S.A. **120**, e2210651120 (2023).

[12] M. Gomez, Ghosts and bottlenecks in elastic snap-through, Ph.D. thesis, University of Oxford, 2018.
[13] D. P. Holmes, Elasticity and stability of shape-shifting structures, Curr. Opin. Colloid Interface Sci. **40**, 118 (2019).
[14] See Supplemental Material at http://link.aps.org/supplemental/10.1103/PhysRevLett.132.267201 for further details of the experimental, numerical and analytical methods, including Refs. [15,16].
[15] Lowess smoothing, https://www.mathworks.com/help/curvefit/lowess-smoothing.html, [Online; accessed 24-May-2024].
[16] B. Audoly and Y. Pomeau, *Elasticity and Geometry: From Hair Curls to the Non-Linear Response of Shells* (Oxford University Press, Oxford, 2010), pp. 205–208.
[17] M. Bergou, M. Wardetzky, S. Robinson, B. Audoly, and E. Grinspun, Discrete elastic rods, ACM Trans. Graph. **27**, 63 (2008).
[18] M. Bergou, B. Audoly, E. Vouga, M. Wardetzky, and E. Grinspun, Discrete viscous threads, ACM Trans. Graph. **29**, 116 (2010).
[19] W. Huang and M. K. Jawed, Newmark-beta method in discrete elastic rods algorithm to avoid energy dissipation, J. Appl. Mech. **86**, 084501 (2019).
[20] R. von Mises, Über die stabilitätsprobleme der elastizitätstheorie, Z. Angew. Math. Mech. **3**, 406 (1923).
[21] S. P. Timoshenko and J. M. Gere, *Theory of Elastic Stabiility* (McGraw-Hill, New York, 1961).
[22] S. H. Strogatz, *Nonlinear Dynamics and Chaos* (Westview Press, Boulder, 2015).
[23] J. Su, The phenomenon of delayed bifurcation and its analyses, in *Multiple-Time-Scale Dynamical Systems*, edited by C. K. R. T. Jones and A. I. Khibnik (Springer, New York, 2001), p. 203.
[24] A. Giudici *et al.*, Transient amplification of pre-existing asymmetries in dynamic snap-through (to be published).